Int. J. Multiphase Flow Vol. 13, No. 3, pp. 387–402, 1987
Printed in Great Britain

0301-9322/87 $3.00 + 0.00
Pergamon Journals Elsevier

AN EXPERIMENTAL STUDY OF 2-D PHASE SEPARATION PHENOMENA

K. M. BUKHARI† and R. T. LAHEY JR
Rensselaer Polytechnic Institute, Troy, NY 12180-3590, U.S.A.

(*Received* 25 *March* 1986; *in revised form* 10 *October* 1986)

Abstract—Experiments were performed to study phase separation and distribution phenomena in a 2-D test section. The conditions tested were intended to simulate the "chimney effect" that may occur during reflood in a pressurized water nuclear reactor (PWR) core after a hypothetical loss-of-coolant accident (LOCA). Such flow situations may enhance the cooling of the higher powered assemblies during reflood.

The countercurrent two-phase flow conditions expected in a PWR were simulated using air/water in a special 2-D test section having two inlet and two outlet ports. The void fraction distribution across the test section was measured with a γ-ray densitometer for different flow conditions, including various flow rates, flow qualities and flow splits between the four ports. These flow conditions were run for cases with and without vertical rods mounted inside the test section. These rods were intended to simulate the effect of the lateral resistance to the flow due to fuel rods in a PWR core. It was found that the presence of the rods dramatically reduced the degree of recirculation observed. A variety of flow regimes were observed, including regions of single-phase water and air, and bubbly, slug and churn–turbulent flows. It is felt that these data form an excellent basis for the assessment of multidimensional two-fluid models of two-phase flow.

INTRODUCTION

Nuclear reactor safety research has dramatically increased our understanding of two-phase flows in the last few decades. However, there are still a number of important problems in two-phase flow that are not well-understood. One such problem is concerned with phase separation and distribution phenomena in channels of complex geometry.

Several previous studies on phase separation have been conducted in branching conduits. Parameters such as the liquid and vapor flow rates, void fraction and pressure distributions have been measured (Honan & Lahey 1981; Saba & Lahey 1984). Mechanistic phase separation models for this geometry have been presented by Saba & Lahey (1984) and Whalley & Azzopardi (1980). It was observed in these test sections that the vapor phase often showed a preference to enter the side branch.

Barasch & Lahey (1981) studied phase separation in a vertical 2-D test section. This test section had a height of 91.44 cm, a width of 30.48 cm and a depth of 1.27 cm. A two-phase mixture consisting of air and water entered the test section from the center of the lower edge of the test section and exited from ports in both sides near the top of the test section. The experiment was performed for several flow rates, with and without vertical stainless-steel (SS) rods inside the test section. These rods simulated the lateral hydraulic resistance to the flow due to fuel rods in a pressurized water reactor (PWR) core. The chordal-averaged and local void fractions were determined as well as the dynamic pressure at a number of locations. It was found that in the absence of the rods there is considerable recirculation within the test section. In contrast, the rods had the effect of limiting recirculation to the lower corner regions.

The test section used by Barasch & Lahey (1981) had an aspect ratio of 1:24 (i.e. ratio of channel depth to channel width). The present study was done using a vertical 91.44 × 91.44 cm channel, of depth 1.27 cm, thus it had an aspect ratio of 1:72. This test section was intended to simulate the so-called "chimney effect" in the core of a PWR during the reflood phase of a loss-of-coolant accident (LOCA). This effect is due to natural circulation due to a vertical upflow of a two-phase mixture in the central part of the core due to boiling-induced bouyancy, and downflow in the peripheral region of the core due to the higher density fluid formed because of heat loss and the

†Current address: Center for Nuclear Studies, P.O. Nilore, Rawalpindi, Pakistan.

lower decay heat in that region. This can result in a countercurrent two-phase flow within the core which can enhance the cooling of the higher powered internal assemblies during reflood.

DISCUSSION

Figure 1 is a photograph of the test section before it was installed in the air/water loop. The two-phase (air/water) inlet was located at the middle of the lower edge of the test section. As shown

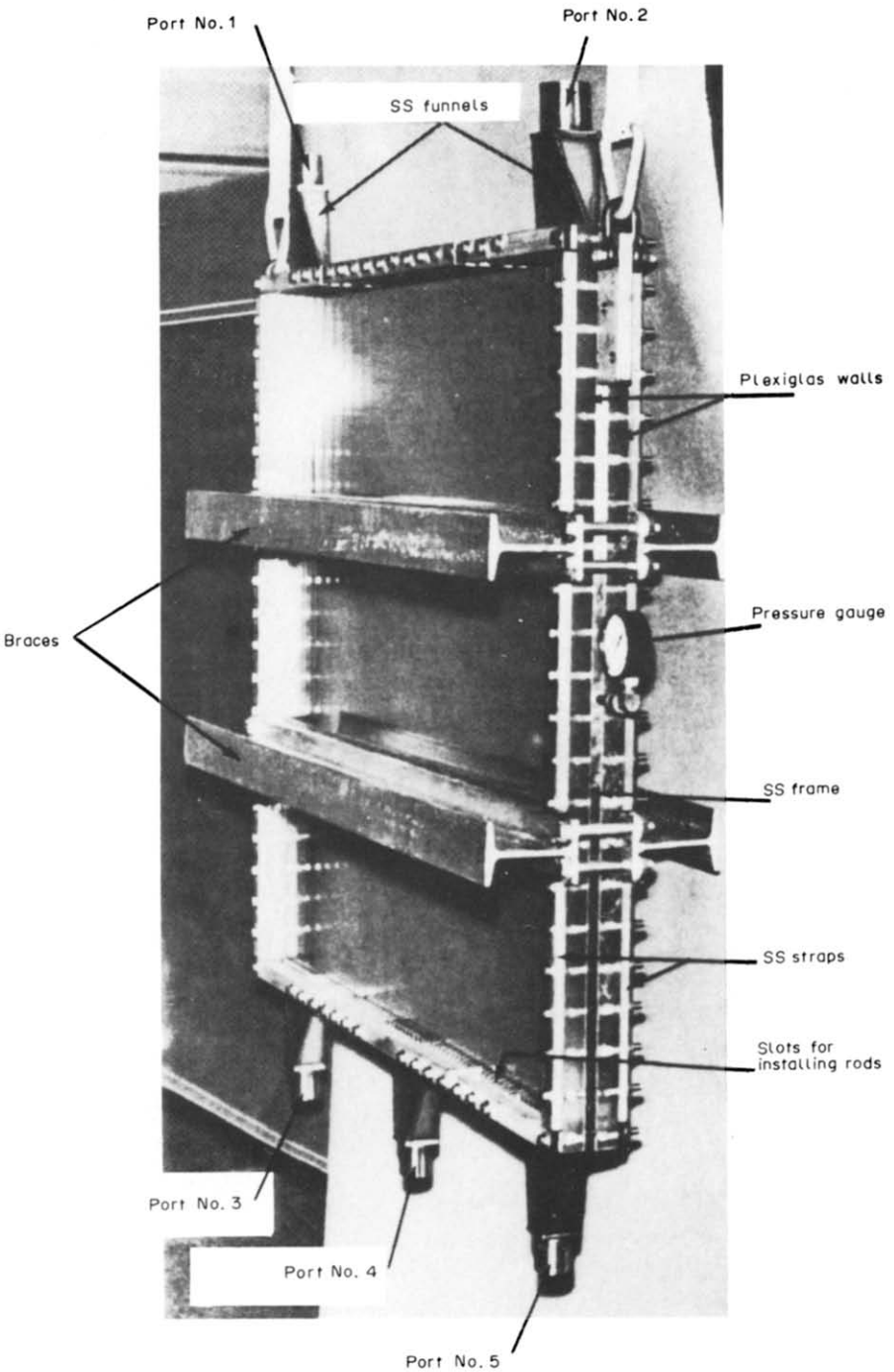

Figure 1. Rear view of the 2-D test section.

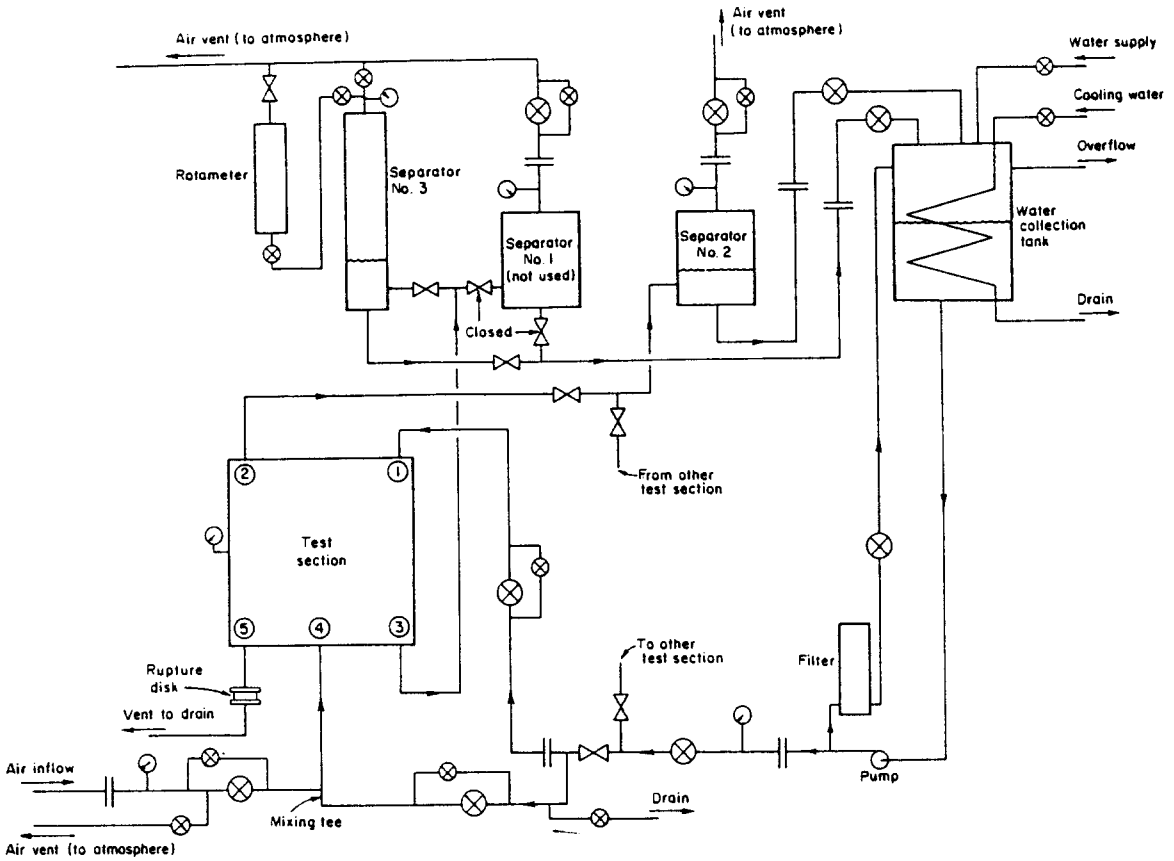

Figure 2. Air/water loop.

in figure 1, this inlet is labeled as port No. 4. Port No. 1 in the top right-hand corner was used as a single-phase water inlet. In addition, there was an outlet in the bottom right-hand corner (port No. 3). In simulating the chimney effect, the two-phase upflow from port No. 2 simulates the upflow in the central part of the core, while the downflow at the right-hand side of the test section simulates the downflow near the core periphery. The exit flow rate from each port was controlled using throttle valves downstream of the phase separators (see figure 2). Finally, port No. 5 was connected to a large-diameter vent pipe through a carbon rupture disk which had a setting of 275 kPa. This was a safety measure to prevent damage to the test section in case of accidental over-pressurization. Port No. 5 could also be used as an alternate location of the inlet port for the two-phase mixture.

A number of different inlet flow conditions were run in the test section. The parameters varied were the air and water flow rates entering the test section, the flow split between port Nos 1 and 4, and the quality of the two-phase flow entering through port No. 4. All of these flow conditions were run with and without the simulated fuel rods in the test section. For each case, the chordal-averaged void fraction profile was determined using a single-beam γ-densitometer, which scanned the test section at three different axial positions.

The large RPI air/water loop shown in figure 2 was used for the conduct of this experiment. This loop has been previously described in detail by Barasch & Lahey (1981), and thus will not be discussed herein.

The Test Section

The test section consisted of an SS frame with a sheet of 2.54 cm thick Plexiglas bolted to it on either side (see figure 1). The frame consisted of four SS bars 1.27 cm thick and 2.54 cm wide welded together to form a square. Five slots, 11.43 cm long and 0.9525 cm wide with radius rounded ends (to make a total length of 11.91 cm) were made in the top and bottom bars to allow the fluid to enter and leave the test section. SS nozzles welded to the frame connected the rectangular slots to the circular piping. The top and bottom sides of the frame also had 0.625 cm wide $\times$ 0.625 cm)

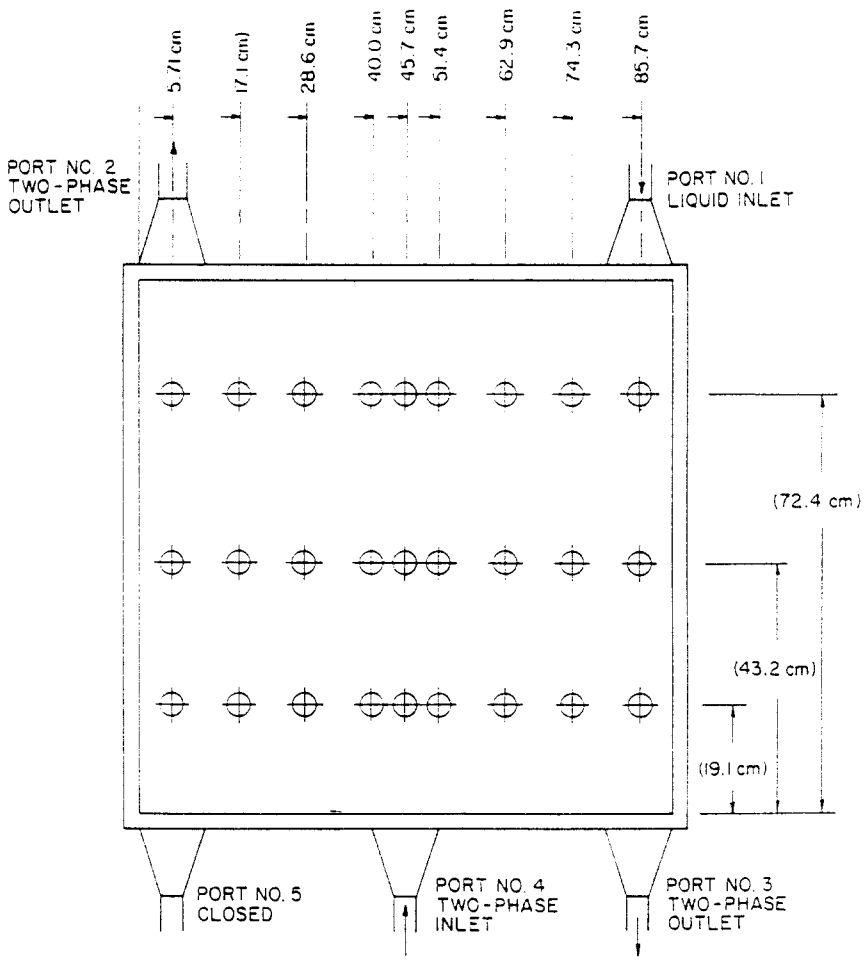

Figure 3. Locations in the test section where the void fraction data was taken.

deep slots in them to accommodate the 0.625 cm dia rods. There were 71 such slots on each side, spaced 1.27 cm (center-to-center) apart. It should be noted that the rod diameter used was smaller than actual PWR rods. This allowed for better flow visualization and void fraction measurements.

Between the frame and the Plexiglas sheets were placed 0.0794 cm thick gaskets to prevent leakage. SS straps were placed on the Plexiglas sheets and bolts were passed through them. In this way, the Plexiglas did not experience high stresses near the bolt holes and the amount of bowing of the test section under pressurization was minimized. As can be seen in figure 1, to further reduce Plexiglas bowing two braces made of steel I-beams, 101.6 cm long, 6.35 cm wide and 10.16 cm high, were placed across the test section on either side, and bolted together, the bolts being outside the test section.

Void fraction data was taken at the 27 locations shown ($\oplus$) in figure 3. When the rods were present, data was taken at 46.4 cm instead of at the centerline (45.7 cm) since a rod was located there. Also, void fraction data was taken at additional points as necessary, based on the visual appearance of the void fraction distribution.

Single-beam γ-Densitometer

The single-beam γ-ray attenuation technique was used to determine the void fraction distribution within the 2-D test section. This technique was used since it is non-obtrusive and its accuracy can be quantified. The physical principle used in this method is that the degree of attenuation of γ-rays on passing through the test section depends, among other things, on the amount of liquid in the ray's path. The chordal average void fraction $\langle\alpha\rangle$, for a well-mixed two-phase flow is given by (Schrock 1969)

$$\langle \alpha \rangle = \frac{\ln\left(\frac{N_{2\phi}}{N_L}\right)}{\ln\left(\frac{N_G}{N_L}\right)}, \quad [1]$$

where $N_{2\phi}$, N_L and N_G are the counts obtained when the γ-beam goes through a two-phase mixture, liquid and vapor, respectively, in a given time interval. To account for the change in detector characteristics due to high voltage drift and changes in room temperature and humidity, a reference count was taken outside the test section before and after each measurement. Thus, we have

$$\langle \alpha \rangle = \frac{\ln\left(\frac{N'_{2\phi}}{N'_L}\right)}{\ln\left(\frac{N'_G}{N'_L}\right)}, \quad [2]$$

where

$$N'_{2\phi} = \frac{N_{2\phi}}{N_{ref}},$$

$$N'_L = \frac{N_L}{N_{ref}}$$

and

$$N'_G = \frac{N_G}{N_{ref}}.$$

The subscript "ref" refers to counts taken outside the test section. By using the normalized counts, $N'_{2\phi}$, N'_G and N'_L, we were able to combine data taken at different times.

The densitometer system used a 5 Ci ^{137}Cs source contained in a cylindrical lead shield that had a collimator on one side. Within the cylindrical shield, the source could be moved and placed directly in front of the collimator hole, such that a γ-ray beam emerges, or it could be moved away from the collimator, in which case it was safely shielded. Details of the shield and collimator design have been given previously by Honan & Lahey (1981).

A detailed error analysis yields

$$\frac{\Delta\langle \alpha \rangle}{\langle \alpha \rangle} = \frac{[2(1 - \langle \alpha \rangle + \langle \alpha \rangle^2)]^{1/2}}{\langle \alpha \rangle \ln\left(\frac{N'_G}{N'_L}\right)} \left[\left(\frac{\Delta N_{2\phi}}{N_{2\phi}}\right)^2 + \left(\frac{\Delta N_{ref}}{N_{ref}}\right)^2\right]^{1/2}, \quad [3]$$

where

$\Delta N_{2\phi}$ = the error in $N_{2\phi}$ (counts when the beam goes through the test section)

and

ΔN_{ref} = the error in N_{ref} (counts at the reference location).

A consideration of the accuracy desired, of the inherent fluctuations in two-phase flow, and of time limitations, led us to choose a counting interval of 6 min. This counting time gives as error of $\Delta\langle \alpha \rangle / \langle \alpha \rangle = \pm 1\%$.

RESULTS

Let us now consider the chordal-averaged void fraction results measured at each location. As can be seen in figure 3, data was taken at three axial positions: 19.1, 43.2 and 72.4 cm, above the inside bottom of the test section. At each axial position, data was taken at no less than nine locations across the test section (as shown in figure 3).

The 36 different flow conditions listed in table 1 were studied. Of these, 18 were with rods and 18 were without rods. For each group of 18 flow conditions, half were at a low liquid flow rate

Table 1. List of all cases run with values of the associated parameters

Figure No.	Case	Symbol in figure	Liquid mass flux (kg/h m^2)	Flow split Port No. 4	Flow split Port No. 1	Quality	Rods in	Pressure (kPa)
4	1AN4	--▽--	0.562E6	50.0%	50.0%	0.3%	No	31.3
4	2AN4	····▽····	0.562E6	50.0%	50.0%	0.6%	No	31.6
4	3AN4	—▽—	0.562ET	50.0%	50.0%	0.9%	No	31.4
5	1BN4	--▲--	0.562E6	62.5%	37.5%	0.3%	No	31.4
5	2BN4	····▲····	0.562E6	62.5%	37.5%	0.6%	No	32.4
5	3BN4	—▲—	0.562E6	62.5%	37.5%	0.9%	No	32.4
6	1CN4	--◇--	0.562E6	37.5%	62.5%	0.3%	No	30.9
6	2CN4	····◇····	0.562E6	37.5%	62.5%	0.6%	No	31.1
6	3CN4	—◇—	0.562E6	37.5%	62.5%	0.9%	No	31.0
7	4AN4	--□--	1.125E6	50.0%	50.0%	0.3%	No	60.2
7	5AN4	····□····	1.125E6	50.0%	50.0%	0.6%	No	63.7
7	6AN4	—□—	1.125E6	50.0%	50.0%	0.9%	No	68.1
8	4BN4	--+--	1.125E6	62.5%	37.5%	0.3%	No	62.7
8	5BN4	····+····	1.125E6	62.5%	37.5%	0.6%	No	67.2
8	6BN4	—+—	1.125E6	62.5%	37.5%	0.9%	No	68.9
9	4CN4	--×--	1.125E6	37.5%	62.5%	0.3%	No	59.5
9	5CN4	····×····	1.125E6	37.5%	62.5%	0.6%	No	61.4
9	6CN4	—×—	1.125E6	37.5%	62.5%	0.9%	No	62.9
10	1AR4	--◆--	0.697E6	50.0%	50.0%	0.3%	Yes	34.5
10	2AR4	····◆····	0.697E6	50.0%	50.0%	0.6%	Yes	33.8
10	3AR4	—◆—	0.697E6	50.0%	50.0%	0.9%	Yes	34.5
11	1BR4	--○--	0.697E6	62.5%	37.5%	0.3%	Yes	34.5
11	2BR4	····○····	0.697E6	62.5%	37.5%	0.6%	Yes	34.5
11	3BR4	—○—	0.697E6	62.5%	37.5%	0.9%	Yes	34.5
12	1CR4	--●--	0.697E6	37.5%	62.5%	0.3%	Yes	33.8
12	2CR4	····●····	0.697E6	37.5%	62.5%	0.6%	Yes	33.8
12	3CR4	—●—	0.697E6	37.5%	62.5%	0.9%	Yes	34.5
13	4AR4	--■--	1.395E6	50.0%	50.0%	0.3%	Yes	75.1
13	5AR4	····■····	1.395E6	50.0%	50.0%	0.6%	Yes	78.1
13	6AR4	—■—	1.395E6	50.0%	50.0%	0.9%	Yes	81.4
14	4BR4	--△--	1.395E6	62.5%	37.5%	0.3%	Yes	76.3
14	5BR4	····△····	1.395E6	62.5%	37.5%	0.6%	Yes	80.5
14	6BR4	—△—	1.395E6	62.5%	37.5%	0.9%	Yes	85.0
15	4CR4	--▼--	1.395E6	37.5%	62.5%	0.3%	Yes	73.5
15	5CR4	····▼····	1.395E6	37.5%	62.5%	0.6%	Yes	78.1
15	6CR4	—▼—	1.395E6	37.5%	62.5%	0.9%	Yes	79.5

and the other half were at a higher flow rate.† For each flow rate, three different flow splits between the two inlet ports Nos 1 and 4 were taken. For each flow split, three different air flow rates entered through inlet port No. 4, giving three different flow qualities.

When the void fraction results are plotted, each case is given a distinct symbol, determined by the shape of the marker representing the data point and by the length of the dashes that make up the line joining the various data points.

Table 1 contains the list of all cases that were run, with the values of liquid mass flux, flow split between port Nos 4 and 1, flow quality at inlet port No. 4, whether the rods were in or not, and the symbol used in plotting them. Figures 4–15 contain plots of the chordal-averaged void fraction distribution. High-speed photographs of some of the instantaneous flow conditions are also shown in figures 16–19. These figures reveal the following.

(*a*) *The flow was recirculating and turbulent*

The general pattern of the directions of motion of the two-phase mixture is shown in figure 20. This figure was made on the basis of photographs and visual inspection of the test section during

†All flow rates are quoted in terms of mass fluxes where the reference was the flow area of the test section.

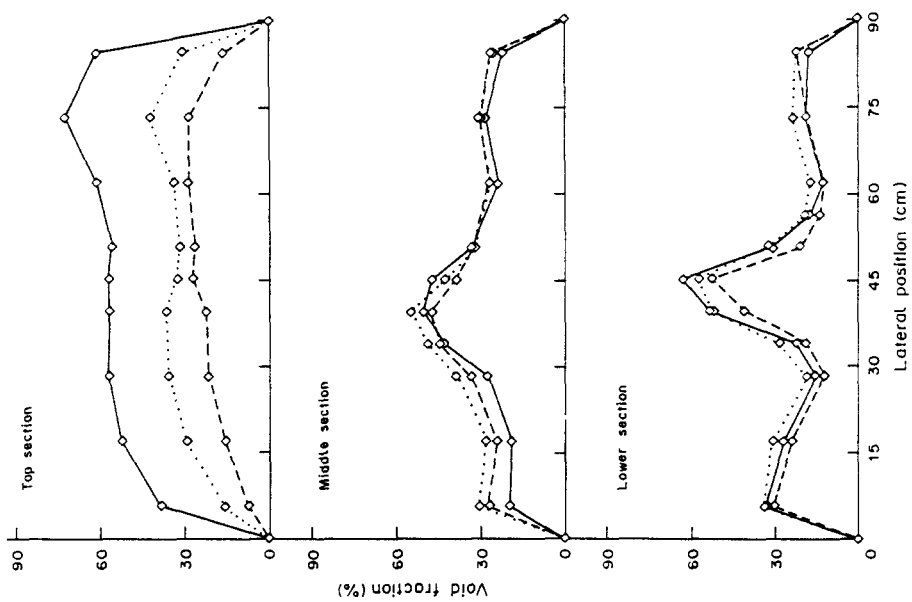

Figure 4. Void fraction for cases 1AN4, 2AN4 and 3AN4. See table 1 for details.

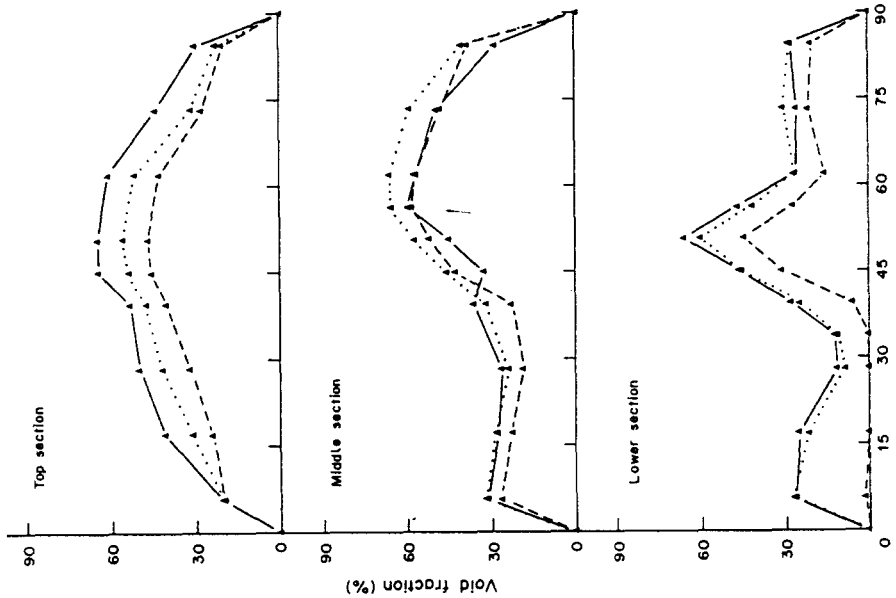

Figure 5. Void fraction for cases 1BN4, 2BN4 and 3BN4. See table 1 for details.

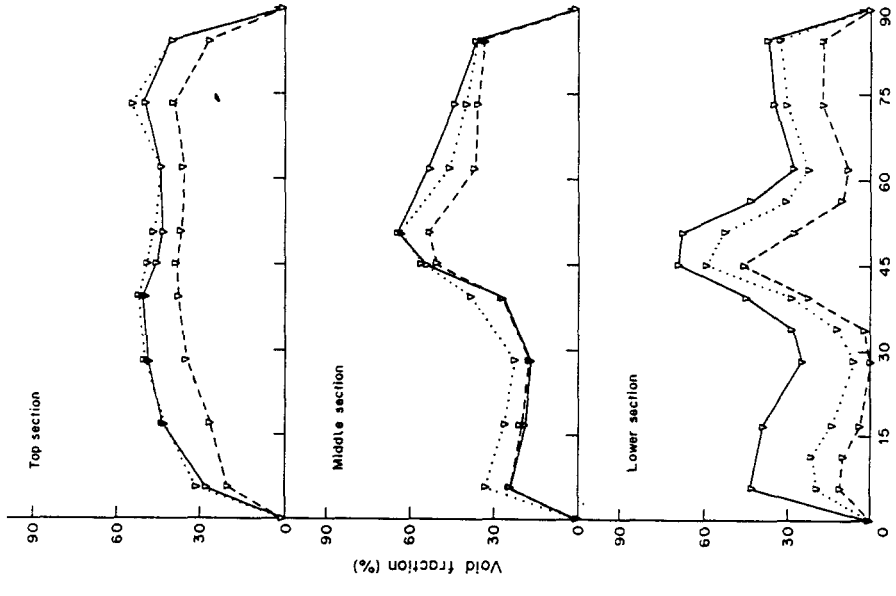

Figure 6. Void fraction for cases 1CN4, 2CN4 and 3CN4. See table 1 for details.

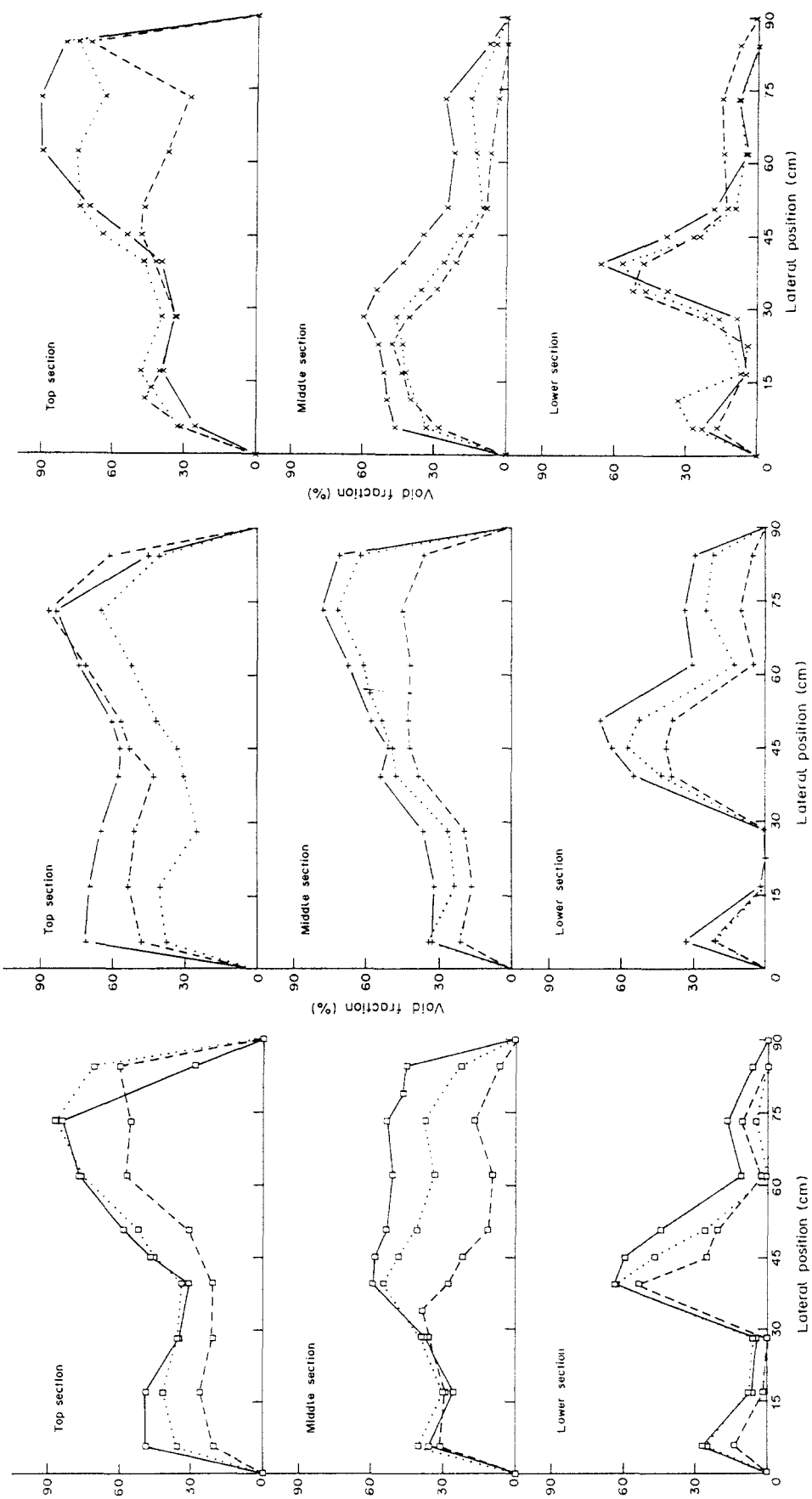

Figure 7. Void fraction for cases 4AN4, 5AN4 and 6AN4. See table 1 for details.

Figure 8. Void fraction for cases 4BN4, 5BN4 and 6BN4. See table 1 for details.

Figure 9. Void fraction for cases 4CN4, 5CN4 and 6CN4. See table 1 for details.

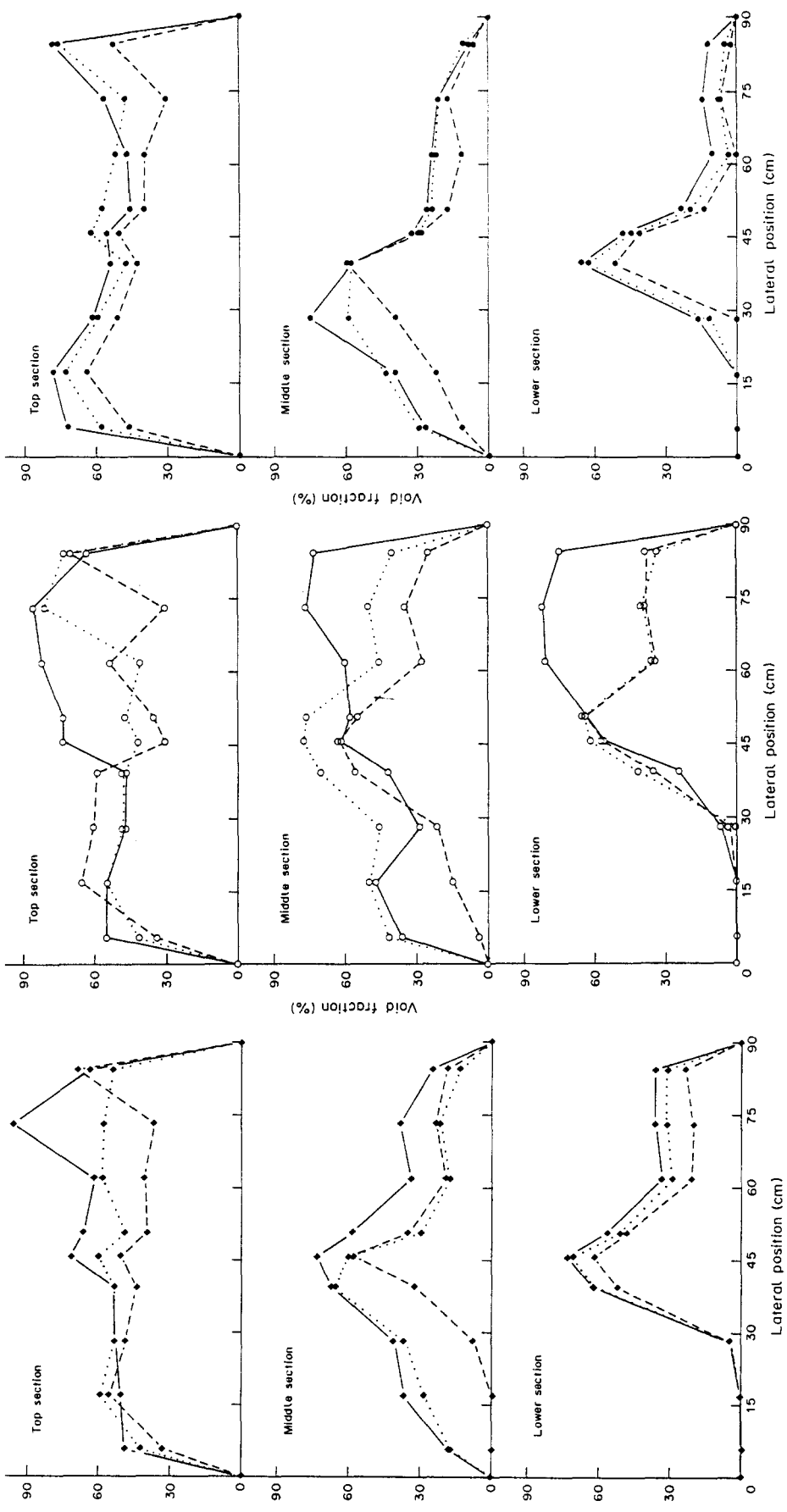

Figure 10. Void fraction for cases 1AR4, 2AR4 and 3AR4. See table 1 for details.

Figure 11. Void fraction for cases 1BR4, 2BR4 and 3BR4. See table 1 for details.

Figure 12. Void fraction for cases 1CR4, 2CR4 and 3CR4. See table 1 for details.

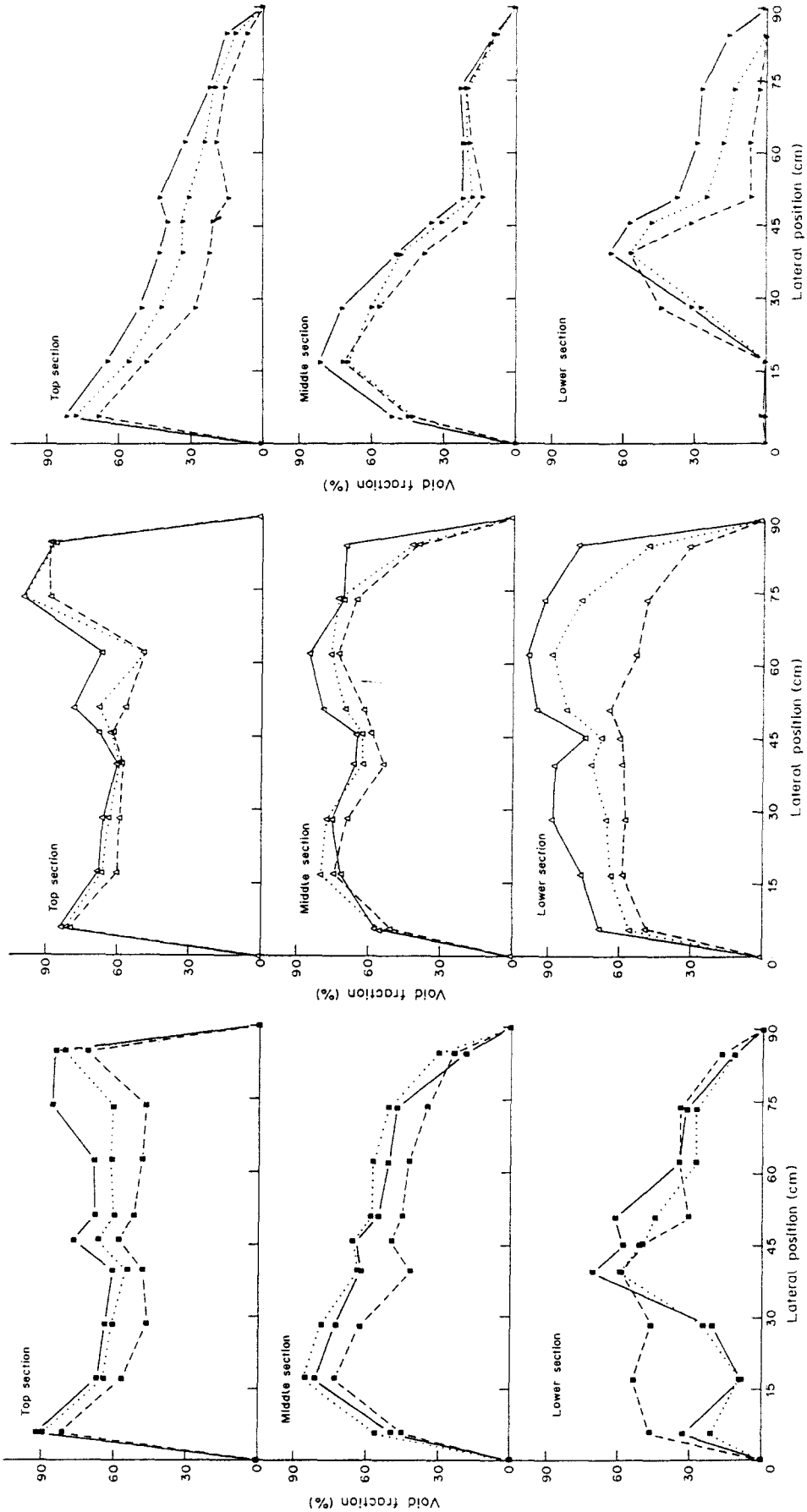

Figure 13. Void fraction for cases 4AR4, 5AR4 and 6AR4. See table 1 for details.

Figure 14. Void fraction for cases 4BR4, 5BR4 and 6BR4. See table 1 for details.

Figure 15. Void fraction for cases 4CR4, 5CR4 and 6CR4. See table 1 for details.

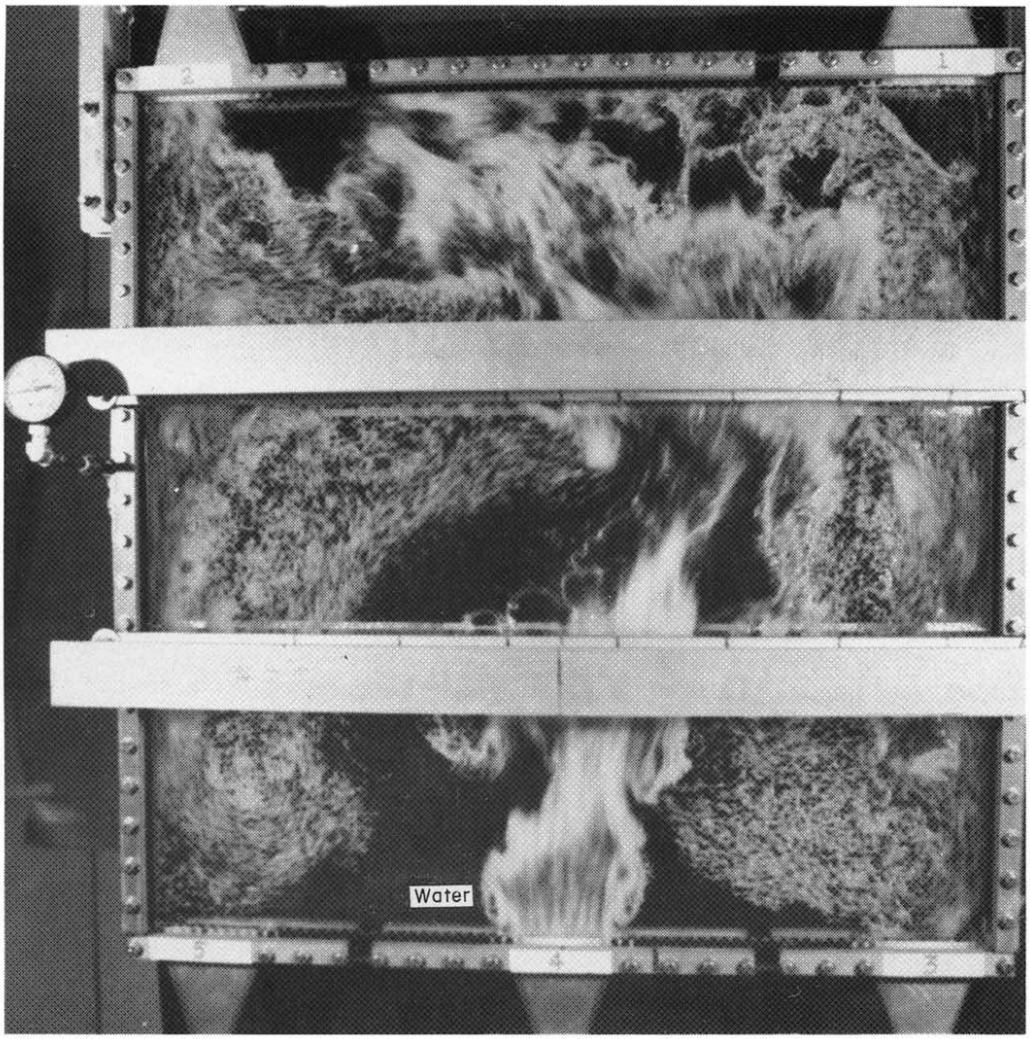

Figure 16. Picture of case 3AN4 (liquid mass flux = 0.562 × 10^6 kg/h m^2, without rods, 50.0/50.0 flow split and quality at inlet No. 4 = 0.9%).

port No. 4. The two-phase mixture entering from port No. 4 shedded vortices just after entering the test section. These were rotating counterclockwise on the left of the inlet and clockwise on the right. A generally similar pattern of flow was observed for the cases when rods were present although the recirculation pattern was suppressed (i.e. the lateral velocities were smaller and there were fewer vortices). The air bubbles also did not reach as low on the left side of the test section as they did in the absence of rods.

(*b*) *There was more than one flow regime in the test section*

The large range of velocities and void fractions present simultaneously in the test section lead to the presence of several flow regimes. For most flow conditions, the phases were distributed in a certain manner in the test section. As can be seen in figure 20, the test section has been divided into eight regions (A–H) based on the visual appearance of the flow. The boundaries between these regions were not as clear-cut as they appear in this figure, and they were constantly fluctuating. Moreover, the size of the regions also depends strongly on the specific flow conditions maintained in the test section. Nevertheless, the regions shown are representative of the flow conditions which occurred during the experiments.

Regions B and D did not contain any air bubbles, rather they were single-phase liquid regions. Region H was an air-pocket having occasional entrained liquid droplets entering it. Much of this

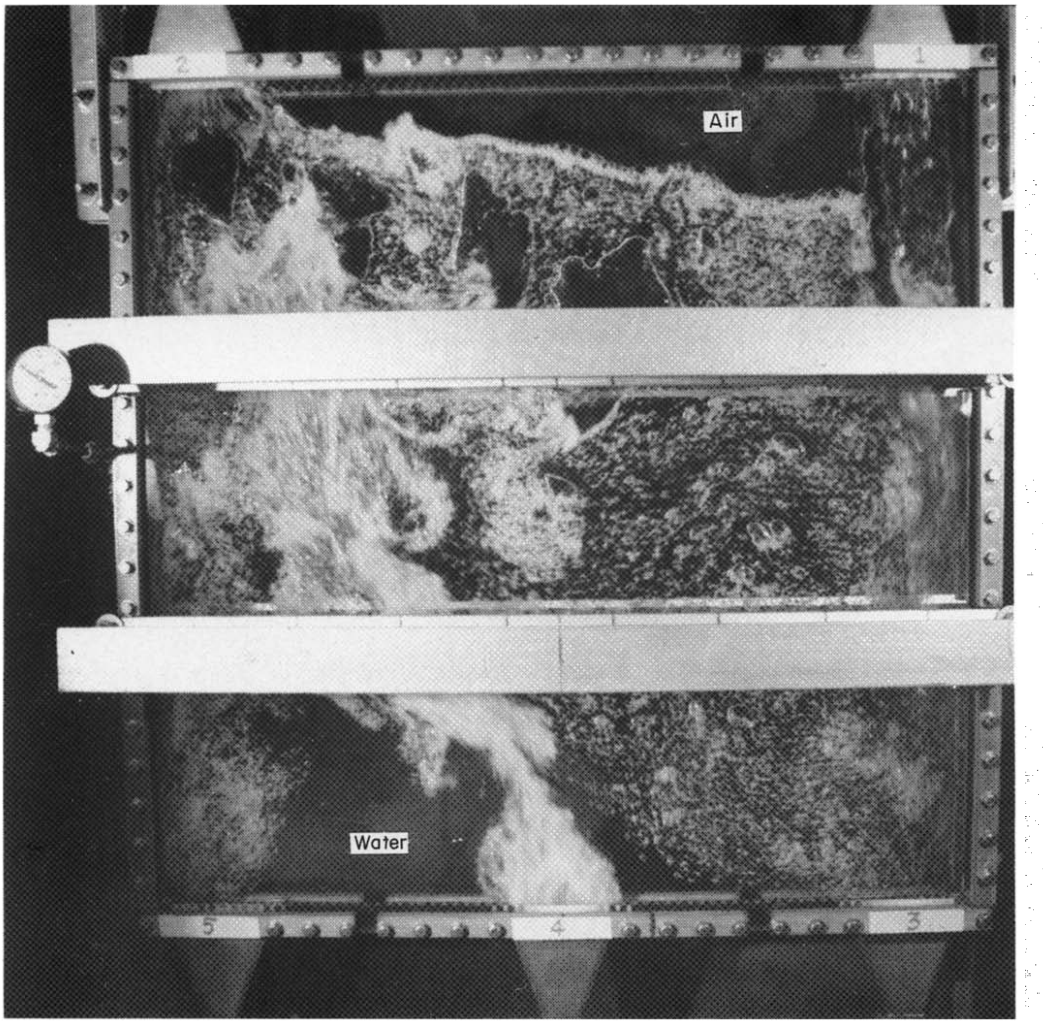

Figure 17. Picture of case 4CN4 (liquid mass flux = 1.125×10^6 kg/h m^2, without rods, 37.5/62.5 flow split and quality at inlet No. 4 = 0.3%).

region remained single-phase throughout the experiments. Region A was generally bubbly flow with the bubble size being approx. 0.6 cm in diameter. Vapor slugs were observed in the upper parts of region A. The flow velocity was too high to observe the flow structure in region C near the inlet, but higher up in region C, the flow was seen to be slug or churn–turbulent. Region E was generally bubbly flow. Region F depended strongly on the flow conditions. For most flow conditions, it was bubbly flow with occasional vapor slugs, especially in its upper region. In cases when the flow split between inlet Nos 4 and 1 was 62.5/37.5 (i.e. a smaller flow entering from port No. 1), region H extended farther down. As the inlet quality increased, region F disappeared and there was a large air space extending down to region E. Liquid droplets entered this air space from region C and fell onto the nearly horizontal air/water interface located inches above the lower edge of the test section. A liquid film flowed down both Plexiglas walls in region H. The resulting higher void fractions in the right-hand side of the test section in the middle and top sections can be seen in figures 5, 8, 11 and 14 (i.e. in all cases with a 62.5/37.5 flow split.)

Region G consisted of water entering from port No. 1. It was mostly pure liquid having a few small entrained air bubbles. Its width depended on the quantity of water entering from port No. 1. These flow regimes generally appeared to be the same for the cases when rods were present, as well as when they were absent. With rods, however, region B is generally larger than without rods,

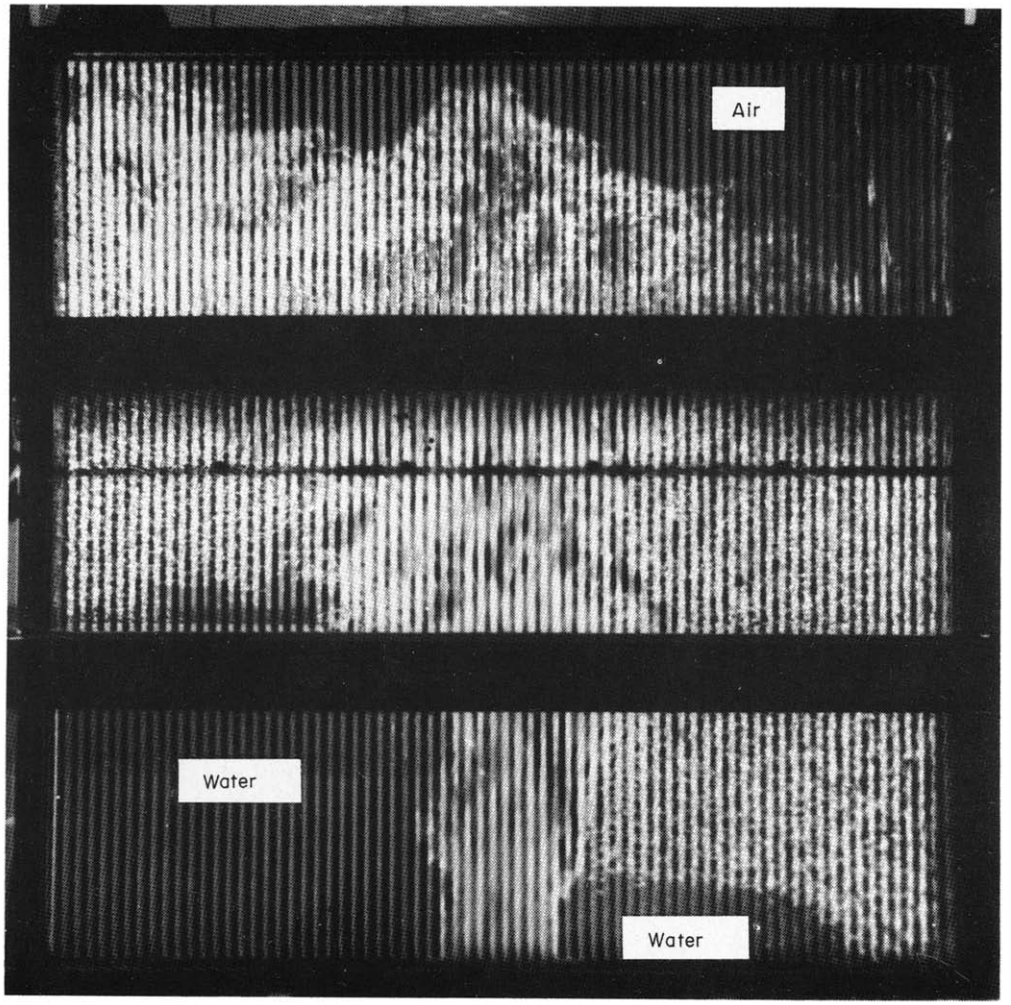

Figure 18. Picture of case 3AR4 (liquid mass flux = 0.697 × 10^6 kg/h m^2, with rods, 50.0/50.0 flow split and quality at inlet No. 4 = 0.9%).

as can be seen from the low void fraction in the lower left-hand corner of the test section in figures 10–12 and 15.

(*c*) *The void fractions depend on flow conditions*

Since data was taken at three axial locations, 19.1, 43.2 and 72.4 cm, above the bottom edge of the test section, most of the present discussion will be limited to these cross sections of the test section.

The effect of inlet flow quality. As can be seen in figures 4–15, an increase in inlet quality generally causes the void fraction to be higher throughout the test section. For cases 1CN4, 2CN4 and 3CN4, it can be seen in figure 6 that the void fractions are similar in the lower and middle sections, but are quite different in the top section. For the high flow, equal flow-split cases (i.e. 4AN4, 5AN4 and 6AN4), figure 7 shows that the void fraction in the right-hand side of the middle section rises sharply as the flow quality increases. In figure 8 this effect is seen for cases 4BN4, 5BN4 and 6BN4, in both the middle and lower sections. The air pocket in these runs came down into the lower section. Cases 4CN4, 5CN4 and 6CN4, are shown in figure 9. In these cases the previously discussed effect is limited to the top section. From these three figures (i.e. figures 7–9), we see that the higher the liquid inflow from inlet port No. 1, the smaller is the size of the air pocket. Alternatively, we note that the higher the total quantity of air through inlet port No. 4, the larger the air pocket in the upper right-hand side. From figures 10–14 a similar trend is seen for the cases when rods

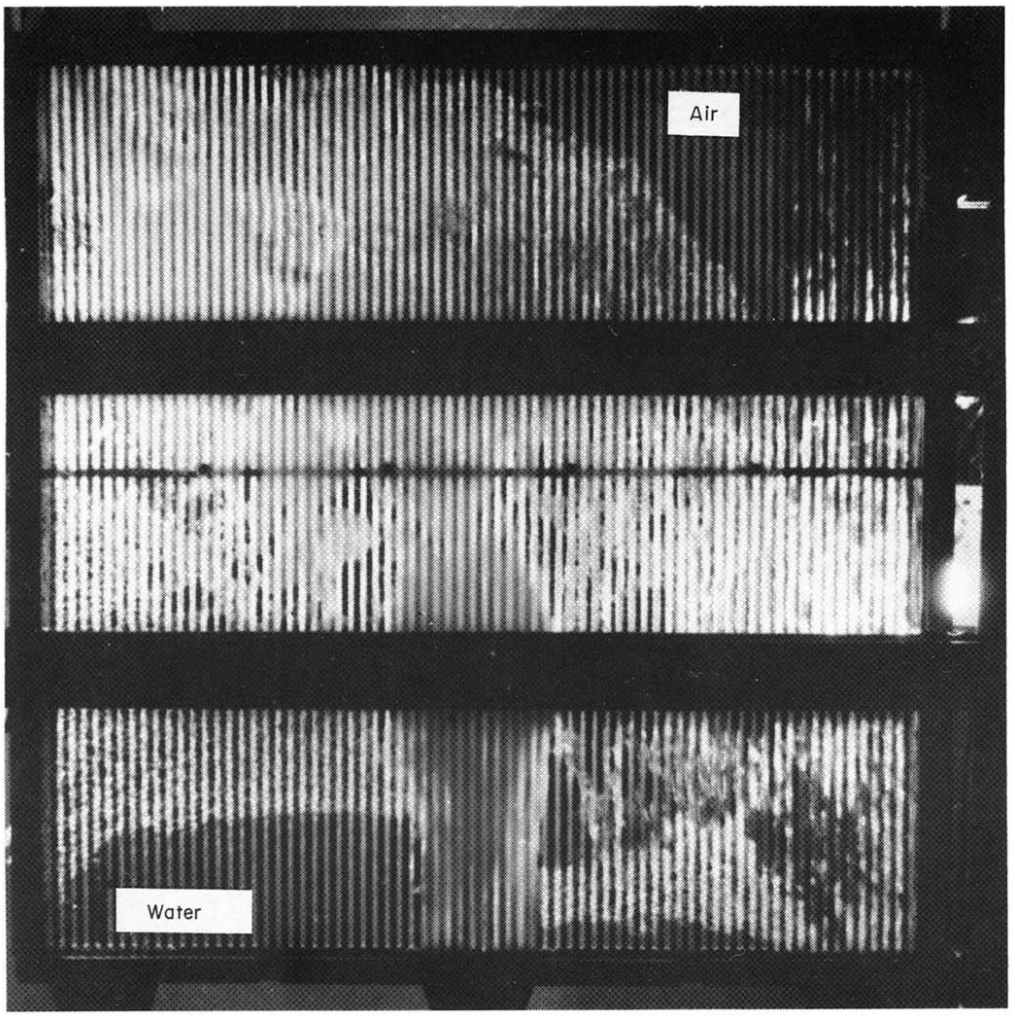

Figure 19. Picture of case 6BR4 (liquid mass flux = 1.395×10^6 kg h m^2, with rods, 62.5 37.5 flow split and quality at inlet No. 4 = 0.9%).

are present. Such a trend is not seen, however, in figure 15 for cases 4CR4, 5CR4 and 6CR4. In these cases, the liquid downflow from port No. 1 was high and a substantial air pocket did not develop. For the cases with rods and low flow rates, shown in figures 10–12, there was a progressive reduction in the size of the single-phase liquid region on the left of inlet No. 4 (i.e. region B in figure 20) with increases in flow quality. For the high-flow cases with rods, this liquid region was almost constant in size.

The effect of flow split. For the case of unequal flow splits between the two inlets, the void fraction was notably higher in one side of the test section. Thus, for all cases with higher inlet flow through port No. 4 than through No. 1 (a 62.5/37.5 flow split), the void fraction was higher in the right-hand side of the test section than in the left-hand side. In cases 4BR4, 5BR4 and 6BR4, the void fraction was high in both sides. This was seen to be the pattern at all three axial sections.

In cases with higher flow through port No. 1 than through port No. 4 (a 37.5/62.5 flow split) the void fraction was higher in the left half of the test section as compared to the right half. These distinctions were more evident in the results for the lower and middle sections. In the top section, the pattern is sometimes reversed: the cases with such flow splits have higher void fraction to the left in cases with rods especially for high flow rates, and slightly to the right for cases without rods, especially at the higher flow rates.

Cases having equal flow split (50/50) between inlet port Nos 4 and 1, do not show such behavior. In the top section, for all such cases, the void fraction is slightly higher in the right side of the test

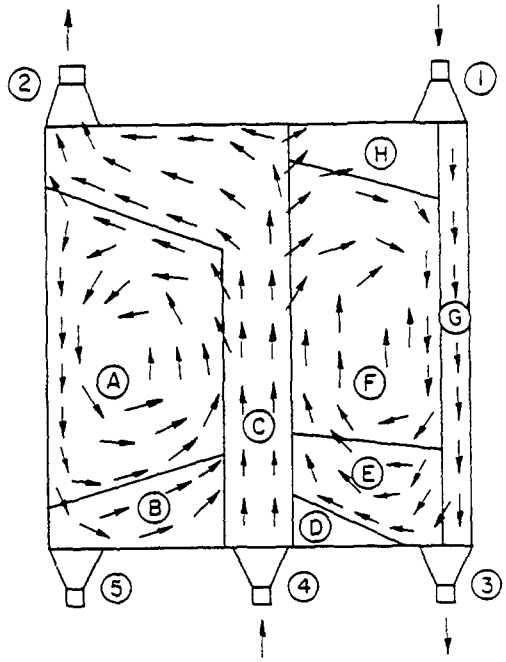

Figure 20. Division of the test section into eight regions based on visual observation of flow regimes (arrows indicate the direction of flow).

the experiments. As seen in figure 20, where the arrows represent the direction of flow, the two-phase mixture moved vertically upwards on entering the test section from port No. 4. On reaching a position near the top edge, most of the flow turned to the left. Of this, a large part exited out of port No. 2, while the rest turned and moved downward along the left edge of the test section. On reaching the bottom of the test section the flow turned to the right and joined the flow coming in from port No. 4. The rest of the flow from inlet No. 4 that had reached the top edge turned to the right and then moved downwards. It mixed with the water coming in from port No. 1 and either went out of exit port No. 3, or turned and joined the two-phase mixture coming in from section than in the left side. In the middle section, it is generally higher to the left than the right except for cases 1AN4, 2AN4 and 3AN4 (i.e. low flow, no rods). In the lower section, it is higher to the right. As seen in figures 4–9, the location where the void fraction is a maximum for cases of equal flow split is generally between the locations where the void fraction peaks for the corresponding cases of the other two flow splits.

The effect of flow rate. For the cases without rods having a 62.5/37.5 flow split, there is no striking difference between the void fraction profiles when the flow rate goes from low to high flow. For cases having a 50/50 flow split, the low-flow cases have a higher void fraction to the right of the test section, while high flow rate caused the void fraction to be higher in the left side of the test section in the lower and middle sections. Near the top section, it was the other way around. A similar effect was seen for a 37.5/62.5 flow split. For all cases involving rods, the void fraction was higher in the test section when the flow rate was higher, especially in the left side of the two-phase inlet in the lower and middle sections.

The effect of rods. We find that the void fraction was normally higher in the presence of rods than without rods. This could be because of homogenization of the flow by the rods, which causes the void fraction to be higher. In contrast, for the high-flow cases with a 37.5/62.5 flow split, the void fraction was higher in the top section in the right-hand side for cases without rods than those with rods. This was due to the absence of the air space (region H of figure 20) when rods were present.

SUMMARY AND CONCLUSIONS

The geometry and flow conditions of this experiment were intended to simulate the so-called PWR "chimney effect" during PWR reflood. The results show that considerable recirculation of

both the liquid and vapor phases can be expected for such conditions. Also, it was noted that several flow regimes were present within the test section at the same time. The presence of rods was found to increase the void fraction, and to reduce the degree of recirculation due to the lateral reistance to the flow caused by the rods.

It is felt that these data form an excellent basis for the assessment of multidimensional two-fluid models of two-phase flow.

REFERENCES

BARASCH, M. & LAHEY, R. T. 1981 The measurement of two-dimensional phase separation phenomena. Report NUREG/CR-1936.

HONAN, T. J. & LAHEY, R. T. 1981 The measurement of phase separation in wyes and tees. *Nucl. Engng Des.* **1,** 93–102.

SABA, N. & LAHEY, R. T. 1984 The analysis of phase separation phenomena in branching conduits. *Int. J. of Multiphase Flow* **10,** 1–20.

SCHROCK, V. W. 1969 Radiation attenuation techniques in two-phase flow measurement. In *ASME Symp. on Two-phase Flow Instrumentation.*

WHALLEY, P. B. & AZZOPARDI, B. J. 1980 Two phase flow in a tee junction. Report AERE-R 9699.